Supporting Information

Symmetry-breaking Actuation Mechanism for Soft Robotics and Active Metamaterials

Shuai Wu[a,1], Qiji Ze[a,1], Rundong Zhang[a], Nan Hu[b], Yang Cheng[c], Fengyuan Yang[c], Ruike Zhao[a,*]

[a]Soft Intelligent Materials Laboratory, Department of Mechanical and Aerospace Engineering, The Ohio State University, Columbus, OH, 43210, USA;

[b]Department of Civil, Environmental and Geodetic Engineering, The Ohio State University, Columbus, OH, 43210, USA;

[c]Department of Physics, The Ohio State University, Columbus, OH, 43210, USA

[1]S. W. and Q. Z. contributed equally to this work.
[*]Correspondence and requests for materials should be addressed to R. Z. (zhao.2885@osu.edu)

Analytical solution for bending and folding behavior of asymmetric and symmetric joints.

As shown in Figure S1, the joint system can be regarded as a two-layer composite beam. The layer on the top is a non-magnetic soft film, with shear modulus G_f, and dimension $L\times W\times T_f$. The layer below is a magnetic unit cell, with shear modulus G_c, and dimension $L\times W\times T_c$. In the analytical study, the ratio between the length L and thickness T_c of the magnetic unit cell is set to be a constant (L/T_c = 10) for convenience. Due to mirror symmetry, only one half of the joint system is investigated. When a magnetic field B is applied perpendicular to the material's magnetization M_c, a deflection υ is induced. Under the small deformation assumption ($\upsilon / L < 0.1$), both materials exhibit linear elastic behavior, and their shear's moduli are one-third of their Young's moduli due to material incompressibility.

To analytically investigate the magnetic driving force that is required to bend or fold the composite beam at the symmetric and asymmetric joints, here, we derive the deflection of the beam as a function of the system's mechanical properties, magnetic properties, and the geometrical dimensions:

$$\upsilon = \upsilon\left(G_f, G_c, T_f, T_c, L, W, M_c, B\right).$$

1. Bending behavior of the asymmetric joint

According to the beam theory, the neutral axis is the location where the normal stress is zero and can be calculated by the stress equilibrium through the cross-section as

$$\sum F_x = \int \sigma dA = \int_{A_c} \sigma_c dA + \int_{A_f} \sigma_f dA = 0, \tag{S1}$$

where σ is the normal stress; A_c and A_f are the cross-section areas of the magnetic unit cell and non-magnetic film, respectively. Recall that the normal stress within the beam is related to the radius of curvature by

$$\sigma = \frac{-3Gy}{\rho}, \tag{S2}$$

where G is the shear modulus of material, y is the distance from a given point to the neutral axis (zero strain axis) shown in Figure S1A, and ρ is the radius of curvature which is a constant at a given cross section. By inserting Eq. S2 into Eq. S1, we obtain

$$3G_c \int_{A_c} y dA + 3G_f \int_{A_f} y dA = 3G_c y_c A_c + 3G_f y_f A_f = 0. \tag{S3}$$

y_c and y_f are the distances from the area centroids of the magnetic cell and film to the neutral axis. Also, the geometric relationship shown in Figure S1A gives

$$y_f - y_c = \left(T_f + T_c\right)/2, \tag{S4}$$

where $T_c = A_c/W$ and $T_f = A_f/W$ are the thicknesses of the magnetic unit cell and non-magnetic film, and W is the width of the system. By combining Eqs. S3 and S4, we can derive the distances between the area centroid and the neutral axis as

$$y_c = \frac{-G_f T_c T_f - G_f T_f^2}{2\left(G_c T_c + G_f T_f\right)}; y_f = \frac{G_c T_c^2 + G_c T_c T_f}{2\left(G_c T_c + G_f T_f\right)}. \tag{S5}$$

Then the moment equilibrium equation at a given cross-section applied with moment τ gives

$$\sum \tau_z = \tau + \int \sigma y dA = \tau + \int_{A_c} \sigma_c y dA + \int_{A_f} \sigma_f y dA = 0, \tag{S6}$$

and using the relationship in Eq. S2, we have

$$\tau = \frac{3G_c}{\rho}\int_{A_c} y^2 dA + \frac{3G_f}{\rho}\int_{A_f} y^2 dA = \frac{3G_c I_c + 3G_f I_f}{\rho}. \tag{S7}$$

When a vertical magnetic field is applied, the magnetic moment $d\tau$ induced in a small volume dV of the beam has the magnitude of

$$d\tau = M_c B dV = M_c BWT_c dx, \tag{S8}$$

where M_c is the magnetization, B is the strength of the uniform magnetic field, and x is the axial direction with $x = 0$ at the free end of the beam. Therefore, the moment distribution along the beam is calculated to be a function of position x as

$$\tau(x) = M_c BWT_c x, \tag{S9}$$

which is equivalent to the moment distribution by applying a point load $P = M_c BWT_c$ at the free end of the beam. Recalling the relationship between the curvature ρ and the deflection υ, and combining Eq. S7, one can obtain

$$\frac{d^2\upsilon}{dx^2} = \frac{1}{\rho} = \frac{\tau(x)}{3G_c I_c + 3G_f I_f}. \tag{S10}$$

By combining Eqs. S9-S10, the deflection along the composite beam for bending behavior can be expressed as

$$\upsilon_{bend} = \frac{M_c BWT_c}{3G_c I_c + 3G_f I_f}\left(\frac{1}{6}x^3 - \frac{1}{2}L^2 x + \frac{1}{3}L^3\right). \tag{S11}$$

By applying the boundary conditions $\upsilon(L) = 0$ and $\upsilon'(L) = 0$, the maximum deflection is then obtained at $x = 0$ (free end of the beam) as

$$\upsilon_{bend}^{\max} = \frac{M_c BWT_c L^3}{9\left(G_c I_c + G_f I_f\right)}. \tag{S12}$$

In addition, according to the parallel axis theorem, the second moment of area to the neutral axis for the magnetic unit cell and film are

$$I_c = I_{\bar{c}} + A_c y_c^2; I_f = I_{\bar{f}} + A_f y_f^2, \tag{S13}$$

where $I_{\bar{c}}$ and $I_{\bar{f}}$ are the second moment of area of the magnetic unit cell and the film to their material centroid, respectively. For rectangle cross-section, the second moment of area is expressed as

$$I_{\bar{c}} = \frac{WT_c^3}{12}; I_{\bar{f}} = \frac{WT_f^3}{12}. \tag{S14}$$

By combining Eqs. S5 and S12-S14, we can derive the maximum deflection of bending at the free end as

$$\upsilon_{bend}^{\max} = \frac{4M_c BL^3\left(G_c T_c^2 + G_f T_f T_c\right)}{3\left[G_c^2 T_c^4 + G_f^2 T_f^4 + 4G_c G_f\left(T_c^3 T_f + T_c T_f^3 + \frac{3}{2}T_c^2 T_f^2\right)\right]}. \tag{S15}$$

Eq. S15 can be rewritten as

$$\upsilon_{bend}^{\max} = \frac{4M_c BL^3\left(\frac{G_c}{G_f}\left(\frac{T_c}{T_f}\right)^2 + \frac{T_c}{T_f}\right)}{3G_f T_f^2\left[\left(\frac{G_c}{G_f}\right)^2\left(\frac{T_c}{T_f}\right)^4 + 1 + 4\frac{G_c}{G_f}\left(\left(\frac{T_c}{T_f}\right)^3 + \frac{T_c}{T_f} + \frac{3}{2}\left(\frac{T_c}{T_f}\right)^2\right)\right]}. \tag{S16}$$

By defining $G_c/G_f = \alpha$, $T_c/T_f = \beta$ and $L/T_c = 10$, we can simplify Eq. S16 as

$$\upsilon_{bend}^{\max} = \frac{400M_c BL\alpha\beta^2\left(\alpha\beta^2 + \beta\right)}{3G_c\left[\alpha^2\beta^4 + 1 + 4\alpha\left(\beta^3 + \beta + \frac{3}{2}\beta^2\right)\right]}. \tag{S17}$$

If we normalize the maximum deflection and the applied magnetic field by

$$\overline{\upsilon_{bend}^{\max}} = \frac{\upsilon_{bend}^{\max}}{L} \text{ and } \overline{B} = \frac{M_c B}{G_c}, \tag{S18}$$

we can further get the relationship between the two dimensionless quantities as

$$\overline{\upsilon_{bend}^{\max}} = \frac{400\alpha\beta^2\left(\alpha\beta^2 + \beta\right)}{3\left[\alpha^2\beta^4 + 1 + 4\alpha\left(\beta^3 + \beta + \frac{3}{2}\beta^2\right)\right]}\overline{B}. \tag{S19}$$

2. Folding behavior of asymmetric and symmetric joints

When the magnetic unit cells fold towards the film direction, the neutral axis (zero-strain axis) is located at the geometric centroid of the film. There exists a film segment with length of 2*l* in between the adjacent magnetic unit cells. As shown in Figure S1B, the magnetic driving force for the folding behavior can be regarded as a moment induced by the magnetic unit cell at $x = L$, which is calculated as $\tau(L) = M_c B W T_c L$. Then the magnitude of deflection and bending angle at $x = L$ are calculated to be

$$\upsilon_{fold}(L) = \frac{\tau(L) l^2}{6 G_f I_f} = \frac{2 M_c B T_c L l^2}{G_f T_f^3}, \tag{S20}$$

$$\theta_{fold}(L) = \frac{\tau(L) l}{3 G_f I_f} = \frac{4 M_c B T_c L l}{G_f T_f^3}. \tag{S21}$$

Based on the geometric relationship of the composite beam as shown in Figure S1B, the maximum deflection of the folding behavior at the free end ($x = 0$) is expressed as

$$\upsilon_{fold}^{\max} = \upsilon_{fold}(L) + \theta_{fold}(L) L = \frac{2 M_c B L^3 T_c \left[\left(\frac{l}{L} \right)^2 + 2 \frac{l}{L} \right])}{G_f T_f^3}. \tag{S22}$$

For the asymmetric joint, we assume the film segment is relatively small ($l = 1/100L$). By substituting $G_c/G_f = \alpha$, $T_c/T_f = \beta$, $L/T_c = 10$ and $l/L = 1/100$, we can simplify Eq. S22 to get the deflection of the folding behavior at the free end as

$$\upsilon_{fold}^{\max} = \frac{200 M_c B L \left(0.01^2 + 0.02 \right) \alpha \beta^3}{G_c}. \tag{S23}$$

With the maximum deflection and the applied magnetic field normalized by

$$\overline{\upsilon_{fold}^{\max}} = \frac{\upsilon_{fold}^{\max}}{L} \text{ and } \overline{B} = \frac{M_c B}{G_c}, \tag{S24}$$

the normalized maximum deflection of folding behavior can be approximated as

$$\overline{\upsilon_{fold}^{\max}} = 4 \alpha \beta^3 \overline{B}. \tag{S25}$$

3. Strain energy of folding and bending behaviors

With the designed asymmetric joint, one system can show asymmetric deflections under switching magnetic field. Also, the energy stored in the system is different for folding and bending behaviors under the same magnitude of field due to the asymmetric deformations. For the two-layer composite beam we discuss above, the internal strain energy in a small volume *dV* is expressed as

$$dU = \frac{1}{2} \sigma \varepsilon dV = \frac{\sigma^2}{6G} dV. \tag{S26}$$

then one can have the total strain energy in the composite beam as

$$U = \frac{1}{6}\left(\int_{V_c} \frac{\sigma_c^2}{G_c} dV + \int_{V_f} \frac{\sigma_f^2}{G_f} dV \right). \tag{S27}$$

For bending behavior, by combining Eqs. S2, S7 and S9, we have

$$\sigma_c = \frac{-G_c M_c BWT_c xy}{G_c I_c + G_f I_f}, \sigma_f = \frac{-G_f M_c BWT_c xy}{G_c I_c + G_f I_f}. \tag{S28}$$

By inserting Eq. S28 into Eq. S27 we can derive the strain energy in the bent composite beam as

$$U_{bend} = \frac{M_c^2 B^2 W^3 T_c^{\,2}}{6\left(G_c I_c + G_f I_f\right)^2} \int_0^L x^2 dx \left(G_c \int_{y_c - T_c/2}^{y_f - T_f/2} y^2 dy + G_f \int_{y_f - T_f/2}^{y_f + T_f/2} y^2 dy \right). \tag{S29}$$

Combining Eqs. S5, S13-S14 and S29 we have

$$U_{bend} = \frac{2M_c^2 B^2 L^3 W^3 T_c^2 \left(G_c T_c + G_f T_f\right)\left[G_c^4 T_c^6 + G_c^3 G_f T_c^3 T_f \left(3T_c^2 + 3T_c T_f + 4T_f^2\right) + 3G_c^2 G_f^2 T_c^2 T_f^2 \left(T_c^2 + 2T_c T_f + 3T_f^2\right) + G_c G_f^3 T_f^5 \left(3T_c - T_f\right) + G_f^4 T_f^6\right]}{3\left(G_c^3 T_c^5 + 5G_c^2 G_f T_c^4 T_f + 6G_c^2 G_f T_c^3 T_f^2 + 4G_c^2 G_f T_c^2 T_f^3 + 4G_c G_f^2 T_c^3 T_f^2 + 6G_c G_f^2 T_c^2 T_f^3 + 5G_c G_f^2 T_c T_f^4 + G_f^3 T_f^5\right)^2}, \tag{S30}$$

which can be simplified as

$$U_{bend} = \frac{2M_c^2 B^2 L^3 W \frac{G_c}{G_f}\left(\frac{T_c}{T_f}\right)^3 \left(\frac{G_c}{G_f}\frac{T_c}{T_f} + 1\right)\left[\left(\frac{G_c}{G_f}\right)^4\left(\frac{T_c}{T_f}\right)^6 + 3\left(\frac{G_c}{G_f}\right)^3\left(\frac{T_c}{T_f}\right)^5 + 3\left(\frac{G_c}{G_f}\right)^3\left(\frac{T_c}{T_f}\right)^4 + 4\left(\frac{G_c}{G_f}\right)^3\left(\frac{T_c}{T_f}\right)^3 + 3\left(\frac{G_c}{G_f}\right)^2\left(\frac{T_c}{T_f}\right)^4 + 6\left(\frac{G_c}{G_f}\right)^2\left(\frac{T_c}{T_f}\right)^3 + 9\left(\frac{G_c}{G_f}\right)^2\left(\frac{T_c}{T_f}\right)^2 + 3\frac{G_c}{G_f}\frac{T_c}{T_f} - \frac{G_c}{G_f} + 1\right]}{3G_c T_c \left[5\frac{G_c}{G_f}\frac{T_c}{T_f} + 6\frac{G_c}{G_f}\left(\frac{T_c}{T_f}\right)^2 + 4\frac{G_c}{G_f}\left(\frac{T_c}{T_f}\right)^3 + 4\left(\frac{G_c}{G_f}\right)^2\left(\frac{T_c}{T_f}\right)^2 + 6\left(\frac{G_c}{G_f}\right)^2\left(\frac{T_c}{T_f}\right)^3 + 5\left(\frac{G_c}{G_f}\right)^2\left(\frac{T_c}{T_f}\right)^4 + \left(\frac{G_c}{G_f}\right)^3\left(\frac{T_c}{T_f}\right)^5 + 1\right]^2}. \tag{S31}$$

By substituting $G_c/G_f = \alpha$, $T_c/T_f = \beta$ and $L/T_c = 10$ into Eq. S31, the total strain energy in the composite beam with bending behavior is expressed as

$$U_{bend} = \frac{200M_c^2 B^2 LWT_c \alpha\beta^3 \left(\alpha\beta + 1\right)\left[\alpha^4\beta^6 + 3\alpha^3\beta^5 + 3\alpha^3\beta^4 + 4\alpha^3\beta^3 + 3\alpha^2\beta^4 + 6\alpha^2\beta^3 + 9\alpha^2\beta^2 + 3\alpha\beta - \alpha + 1\right]}{3G_c\left(5\alpha\beta + 6\alpha\beta^2 + 4\alpha\beta^3 + 4\alpha^2\beta^2 + 6\alpha^2\beta^3 + 5\alpha^2\beta^4 + \alpha^3\beta^5 + 1\right)^2}. \tag{S32}$$

Here, we define the magnetic potential U_{mag} as the work required to align the magnetic unit cell's magnetization with the applied magnetic field, and it is calculated as $U_{mag} = M_c BWT_c L$. We can then normalize the strain energy by the magnetic potential as

$$\overline{U}_{bend} = \frac{U_{bend}}{U_{mag}} = \frac{U_{bend}}{M_c BWT_c L}. \tag{S33}$$

The relationship between the normalized strain energy and the normalized applied magnetic field can be derived explicitly as

$$U_{bend}=\frac{200\alpha\beta^3\left(\alpha\beta+1\right)\left[\alpha^4\beta^6+3\alpha^3\beta^5+3\alpha^3\beta^4+4\alpha^3\beta^3+3\alpha^2\beta^4+6\alpha^2\beta^3+9\alpha^2\beta^2+3\alpha\beta-\alpha+1\right]}{3\left(5\alpha\beta+6\alpha\beta^2+4\alpha\beta^3+4\alpha^2\beta^2+6\alpha^2\beta^3+5\alpha^2\beta^4+\alpha^3\beta^5+1\right)^2}\overline{B}. \quad \text{(S34)}$$

When the magnetic unit cells fold towards the film's direction, we assume the strain is only developed in the short segment of film (l <x< L)at the asymmetric joint, while the magnetic unit cell only undergoes rigid body rotation, thus we can have the strain energy of the system as

$$U_{fold}=\int_{V_f}\frac{\sigma_f^2}{6G_f}dV=\int_{V_f}\frac{\tau^2y^2}{6G_fI_f^2}dV=\int_L^{L+l}\frac{\tau^2}{6G_fI_f}dx, \quad \text{(S35)}$$

in which the moment $\tau = M_cBWT_cL$ is a constant for l <x< L. The strain energy of folding behavior can be calculated as

$$U_{fold}=\frac{M_c^2B^2W^2T_c^2L^2l}{6G_f\frac{WT_f^3}{12}}=\frac{M_c^2B^2W^2T_c^2L^2\frac{L}{100}}{\frac{WG_cT_c^3}{2\alpha\beta^3}}=\frac{2\alpha\beta^3M_c^2B^2WT_cL}{G_c}, \quad \text{(S36)}$$

then the normalized strain energy of folding behavior is expressed as

$$\overline{U}_{fold}=\frac{U_{fold}}{U_{mag}}=\frac{U_{fold}}{M_cBWT_cL}=\frac{2\alpha\beta^3M_cB}{G_c}=2\alpha\beta^3\overline{B}. \quad \text{(S37)}$$

Calculation of the effective stiffness of the magnetic-actuated metamaterial

The demonstration of the 2D multimodal deformation shown in Fig. 6 in the main text has shown great potential in designing active metamaterial with tunable properties. Here, to illustrate the tunable mechanical property that is achieved by the well-controlled external magnetic field, we evaluate the effective stiffness of the magnetic-actuated structures with the initial geometries shown in Figures 6A & G (shown again in Figures S2A & D) under an applied magnetic field B. During magnetic actuation, the system deforms to a geometry which can be regarded as a square with effective dimensions of L×L. When the deformed system is subject to a displacement-controlled loading Δ to both top vertices, the resultant compressive nominal stress S is calculated from the measured total reaction force P and defined as

$$S=P/LW, \quad \text{(S38)}$$

where W is the out-of-plane width of the system. The compressive strain is calculated as

$$\varepsilon=\Delta/L. \quad \text{(S39)}$$

The relationships between the compressive nominal stress and the strain are plotted in Figures S2C & F, and the effective stiffnesses are calculated as the initial slope of each loading curve:

$$K=S/\varepsilon=P/\left(\Delta\cdot W\right). \quad \text{(S40)}$$

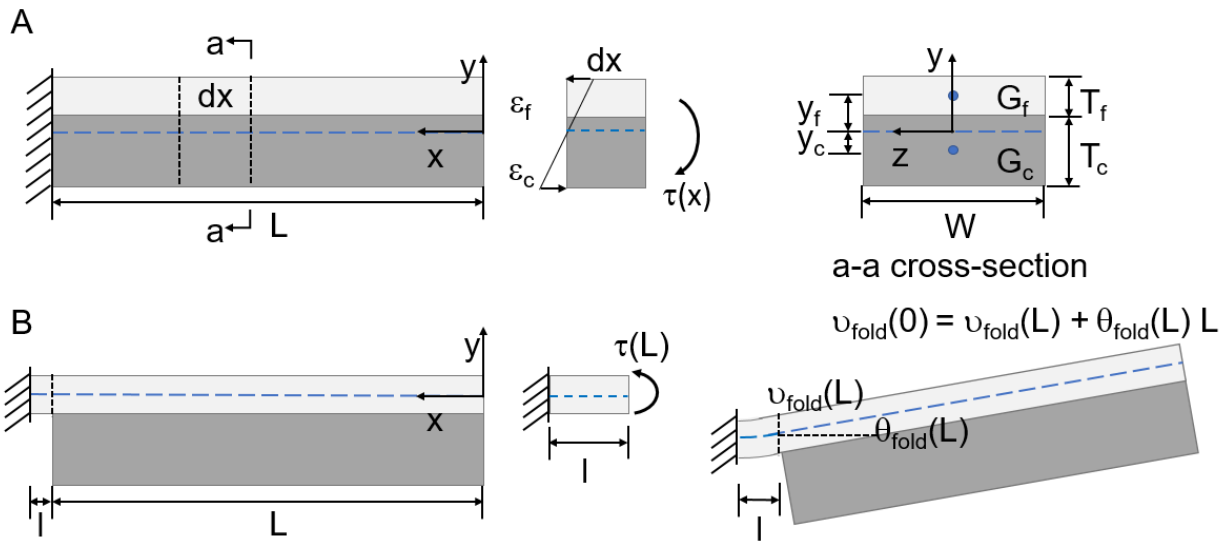

Figure S1. Half model of a two-layer composite beam with an asymmetric joint. (*A*) Dimensions and boundary condition of a bent composite beam. (*B*) Dimensions, boundary condition and geometric relationship of a folded composite beam.

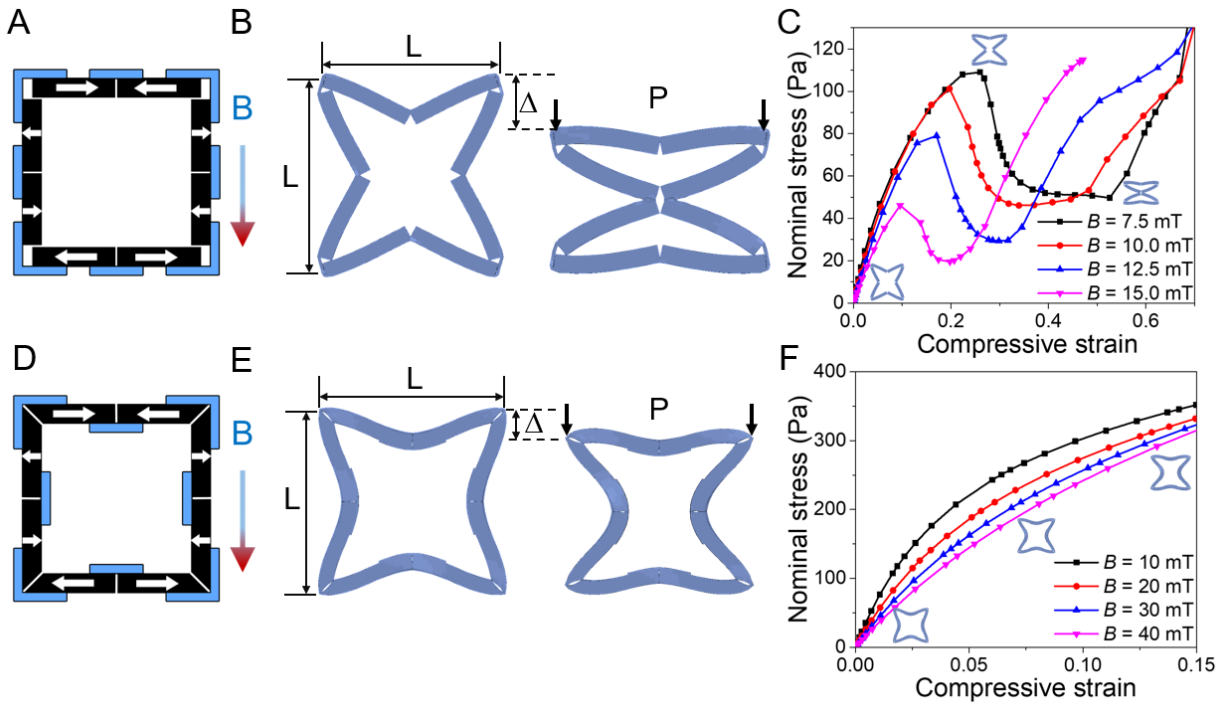

Figure S2. Calculation of the effective stiffnesses of the 2D multimodal systems. (*A*-*C*) A square ring with outside joints. (*A*) Schematic geometry and magnetizations, (*B*) loading condition and (*C*) nominal stress with respect to compressive strain, (*D*-*F*) A square ring with alternating inside and outside joints. (*D*) Schematic geometry and magnetizations, (*E*) loading condition and (*F*) nominal stress with respect to compressive strain.

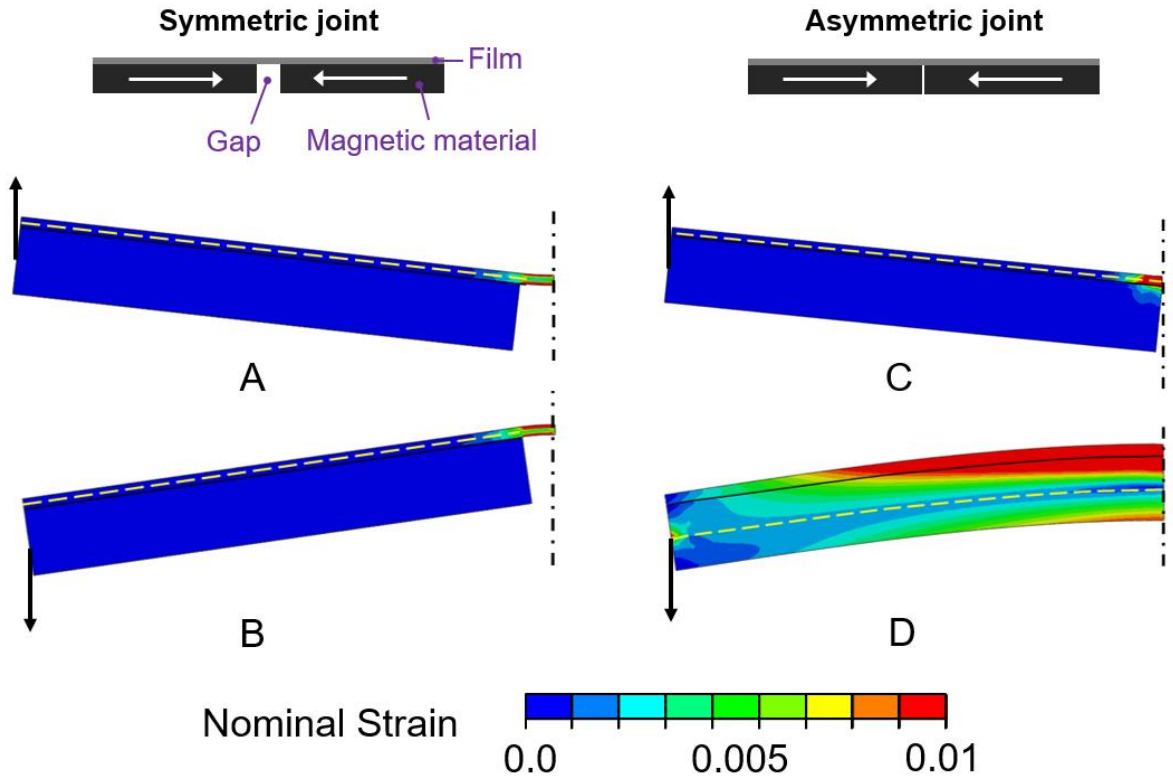

Figure S3. Simulations of a two-layer composite beam bending with either a symmetric joint or an asymmetric joint under a point load at the free-end with mirror symmetry condition. (*A*-*B*) The obtained bending stiffnesses of the beam with symmetric joint are both 0.5×10^{-2} N/m for (*A*) & (*B*). (*C*-*D*) The bending stiffnesses of the beam with asymmetric joint are 5.8×10^{-2} N/m for folding in (*C*), and 2.3 N/m for bending in (*D*). The bending stiffness is calculated as dividing the point load by the free-end deflection ($K = P/\upsilon$). Small deformation assumption is ensured by limiting the deflection within 0.1 time of the beam length ($\upsilon \leq 0.1L$). Contour shows nominal strain. Dashed lines indicate the neutral axis with zero strain.

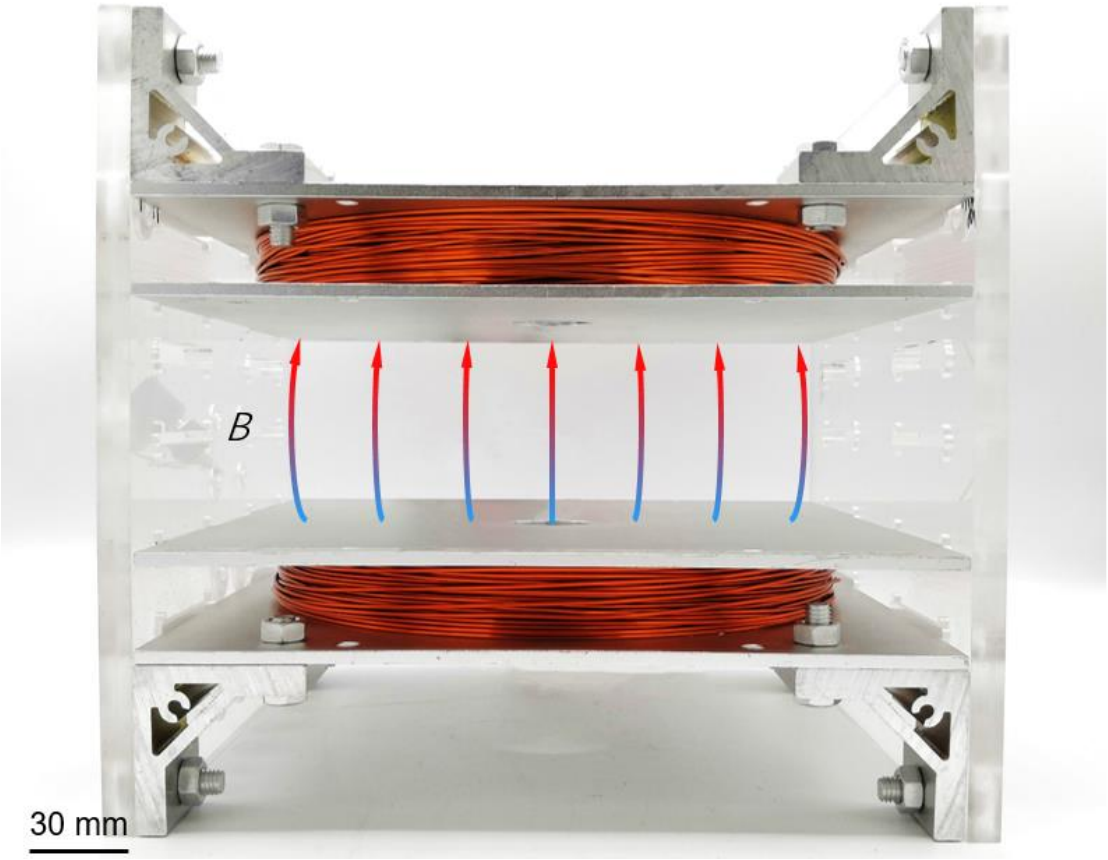

Figure S4. Image of the single-axis Helmholtz coils for generation of 1D magnetic field *B* with controllable magnitude and frequency.

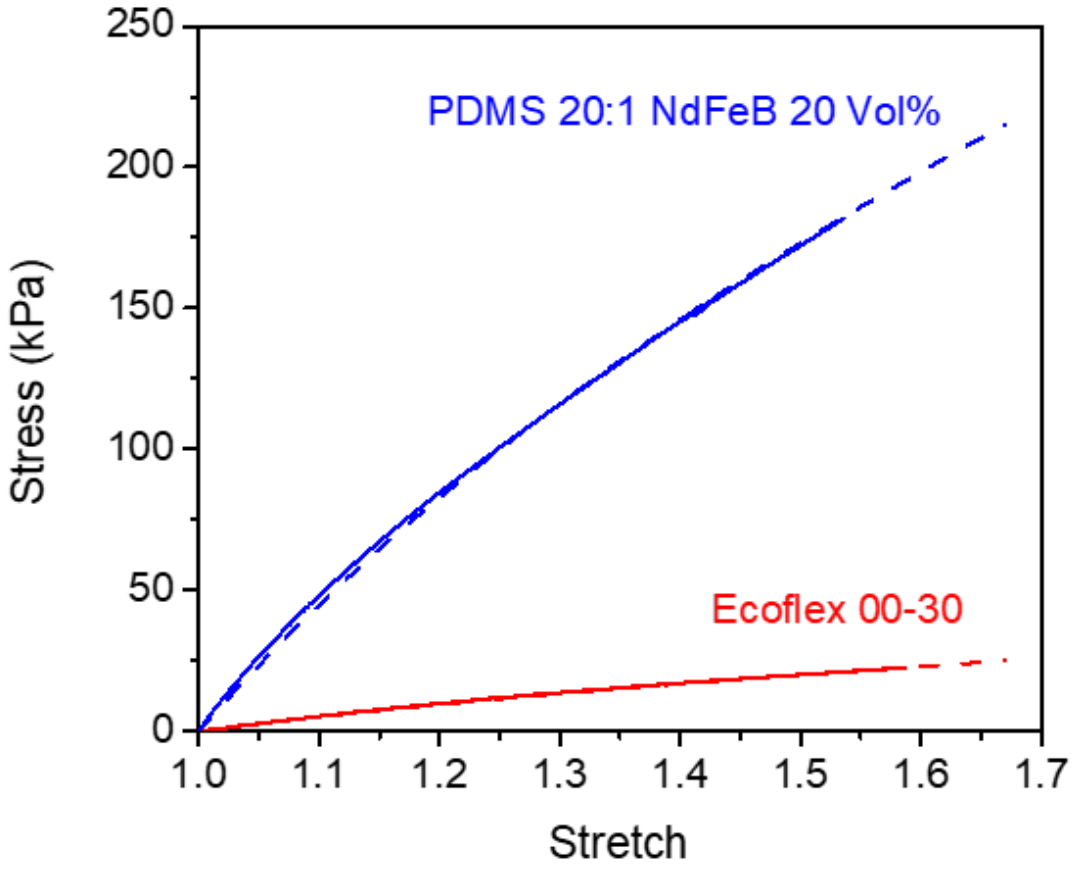

Figure S5. Mechanical characterization of materials used for demonstrations in the paper. Blue curves: Magnetic PDMS; red curves: non-magnetic Ecoflex. The solid and dashed curves represent experimental and fitting curves. The shear moduli of magnetic PDMS and Ecoflex are 164 kPa and 19 kPa, respectively.

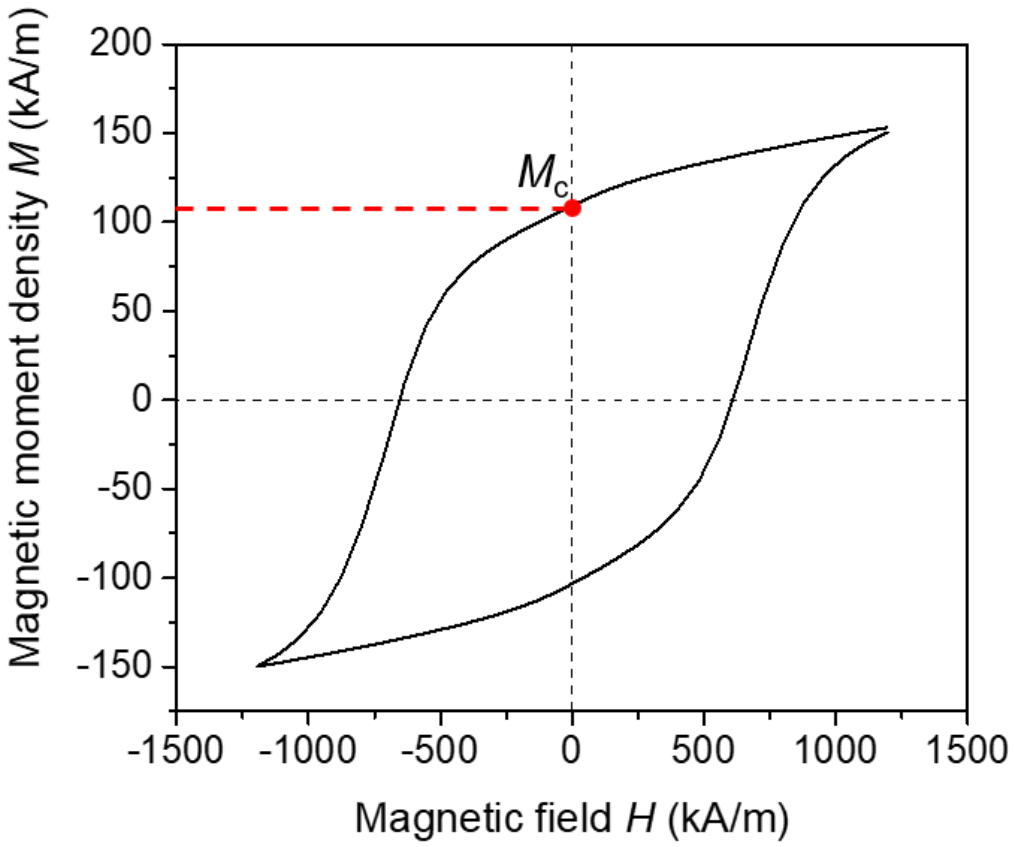

Figure S6. Vibrating Sample Magnetometer (VSM) measurement of magnetic hysteresis loop of magnetic PDMS. The material is composed of PDMS (weight ratio of base and curing agent is 20:1) and NdFeB particles with 20% volume fraction. The remnant magnetization of the magnetic cell M_c is 109 kA /m, as indicated by the red dot in the figure.

Supporting Video Captions

Video S1. Magnetic-actuated 1D multimodal deformation for the four-cell systems (mp4).

Video S2. Magnetic-actuated 1D multimodal deformation for the eight-cell system (mp4).

Video S3. Magnetic-actuated crawling robots (mp4).

Video S4. A four-leg biomimetic swimming robot with multimodal deformation (mp4).

Video S5. Comparison between the biomimetic swimming robot with multimodal deformation and the control case with bending-only deformation (mp4).

Video S6. Magnetic-actuated 2D multimodal deformation (mp4).

Video S7. Magnetic-actuated metamaterial systems (mp4).

References

1. Zhao, R.; Kim, Y.; Chester, S. A.; Sharma, P.; Zhao, X. Mechanics of Hard-Magnetic Soft Materials. *J. Mech. Phys. Solids* 2019, 124, 244−263.
2. Kim, Y.; Yuk, H.; Zhao, R.; Chester, S. A.; Zhao, X. Printing Domains for Untethered Fast-Transforming Soft Materials. *Nature* 2018, 558, 274−279.